Determination of Oxygen Diffusion and Surface Exchange Coefficients of Mixed Ionic-Electronic Conductors by Oxygen Semi-Permeation Methods

Pierre-Marie Geffroy, Eva Deronzier, Jean Gillibert, Pascal Munch, Thierry Chartier, Jacques Fouletier

Determination of oxygen diffusion and surface exchange coefficients of mixed ionic-electronic conductors by oxygen semi-permeation methods

Pierre-Marie Geffroy[a], Eva Deronzier[a], Jean Gillibert[b], Pascal Munch[a], Thierry Chartier[a], Jacques Fouletier[c]*

[a] IRCER, CNRS, Université de Limoges, CEC, 12 Rue Atlantis 87068 Limoges, France

[b] University of Orléans, PRISME EA 4229, Orléans 45000, France

[c] Univ. Grenoble Alpes, Univ. Savoie Mont Blanc, CNRS, Grenoble INP, LEPMI, 38000 Grenoble, France

KEYWORDS: oxygen semi-permeation, mixed ionic-electronic conductors, oxygen diffusion coefficient, surface exchange coefficients.

ABSTRACT: The understanding of oxygen transport mechanisms through mixed ionic-electronic conductors is of great interest for the development of electrochemical devices at high temperature for energy conversion applications. This study is focused on the determination of two coefficients — the oxygen diffusion coefficient and the surface exchange coefficient which are key parameters for the electrochemical performance of a material. These coefficients can be largely impacted by the measurement conditions. The oxygen semi-permeation method is an adequate method to determine these two fundamental coefficients close to the working conditions of the material, i.e., under small or large oxygen partial pressure gradients.

1. INTRODUCTION

Recent developments in solid oxide fuel cells (SOFCs) operating at low temperatures (500-600°C), solid oxide electrolyzer cells (SOECs), and oxygen transport membranes (OTMs) are largely based on the use of mixed ionic-electronic conductors (MIECs)[1-10]. Modeling the transfer process through an MIEC is an important challenge for improving oxygen transport membranes[11-14], reducing the source of error in devices (oxygen sensors, high-temperature fuel cells, and electrolyzers)[15-18], and for developing methods to characterize the transport properties in oxides (emf technique and Faradaic efficiency method)[19-23].

Since the pioneering work of Wagner[24-26], substantial effort has been devoted to modeling oxygen permeation through a mixed ionic-electronic conductor (MIEC). It is now admitted that the oxygen permeation flux is simultaneously controlled by the bulk diffusion and surface exchange for most OTM materials. With a mixed regime, it is difficult to obtain an explicit relationship between the oxygen flux, rate constants of the steps involved in the permeation process, and the actual partial pressures on both sides of the membrane. It is generally not easy to determine kinetic parameters in conditions that are close to the working conditions, i.e., in very small or very high oxygen potential gradients through the membrane, or at low or very high temperatures, etc.

Transport across a semipermeable membrane is commonly described by two parameters: the bulk diffusion coefficient and the surface exchange coefficient. These coefficients are usually determined experimentally by applying one of the following driving forces to the studied oxide: electrical potentia1 gradient, isotopic tracer concentration gradient, or chemical potential gradient. In this work, the bulk diffusion coefficient and the surface exchange coefficient are noted as following: D_O and k are determined by semi-permeation method, D* and k* are determined under

isotopic tracer concentration gradient, D_{chem} and k_{chem} are determined under chemical potential gradient or by electrical conductivity relaxation (ECR) method, as reported previously by Maier[27].

Bouwmeester et al. proposed a characteristic thickness L_c, with $L_c = D^*/k^*$, to provide an estimation for whether the bulk diffusion or the surface exchange dominates the oxygen transport through the oxides; in other words, for a membrane thickness L equal to L_c, the total driving force is equally distributed through the bulk and at the oxide–gas interface[28,29]. When the sample thickness, L, is much larger than L_c, the oxygen transport is limited by diffusion in the bulk, and for L values much smaller than L_c, the oxygen transport is limited by surface exchange kinetics[30]. It should be recalled that the expression for L_c ($L_c = D^*/k^*$) has been established with assumptions, i.e., that the oxide exhibits a predominant electronic conduction, the oxygen pressure gradient across the membrane is small, and the oxygen flux is proportional to the oxygen pressure gradient across both interfaces. Bouwmeester et al. have collected L_c values reported by various authors for a number of perovskite-type oxides[28]. For most perovskite oxide materials, the L_c has a value of approximately 100 μm. The validity of this parameter will be discussed below (Section 2.2), because it must be considered as an indicator.

There are three primary experimental methods used to simultaneously evaluate the oxygen diffusion coefficient through the membrane and the kinetics of oxygen exchange at the surface of a studied mixed conductor: the isotopic exchange depth profile (IEDP) method, with secondary ion mass spectrometry (SIMS)[31-36], the electrical conductivity relaxation method (ECR)[37-46], and the oxygen permeation measurement[11,28,30,47-49]. Additionally, two of these techniques could be used in combination[47,50]. More recently, the effect of applying an overpotential to the oxygen isotope exchange and diffusion in oxide thin film electrodes has been investigated[51]. An oxygen

stoichiometry re-equilibration method under reducing conditions using solid electrolyte coulometry[52] or a thermogravimetric relaxation technique[53] has also been proposed.

The IEDP method extracts the D* and k* values from fitting the isotopic penetration depth profile in the solid from the solution of Fick's second law with appropriate boundary conditions[54]. As recalled by Kan[55], the sample is considered in equilibrium with the gas phase; consequently, it is not possible to study any charge transfer step(s) with this technique.

More recently, temperature-programmed experiments based on isotopic ^{18}O exchange processes, referred to as isothermal isotopic exchange (IIE), have been proposed[55-57]. The main difference from IEDP is that the experiment is conducted *in-situ* with powder samples; in these conditions the process can be considered as surface limited. Bouwmeester et al.[58-60] proposed a pulse-response ^{18}O–^{16}O isotope exchange (PIE) technique based on isotopic analysis of an ^{18}O-enriched gas phase pulse after passage of a continuous flow packed-bed microreactor loaded with the oxide powder.

Another way to estimate the surface exchange coefficient is to use the MIEC as electrode on a solid electrolyte[61]. Using current density–overpotential curves or impedance spectroscopy technique, the exchange current density i_o can be determined (see, as an example,[61]). It is generally admitted that i_o is proportional to the surface exchange coefficient obtained by the isotopic exchange method, according to[62,63]:

$$i_o = 2\,F\,k^*\,C_O \qquad (1)$$

where F is the Faraday constant, and C_O is the bulk concentration of oxide ions in the MIEC. However, the values of i_o calculated by both methods are often not identical[62]. According to Mogensen et al.[63], a conversion factor of the order of $2.\ 10^4$ between k and i_o may be used for oxide materials having a fluorite structure, and of $1.5.\ 10^4$ for perovskite structures. Methods based on

electrochemical impedance spectroscopy to determine oxygen diffusion and surface exchange coefficients in porous perovskite materials taking into account the microstructure, i.e., porosity, tortuosity, and surface area, have also been proposed[64-65].

The oxygen surface exchange coefficient has been also measured using a bilayer curvature relaxation technique, with the advantage of allowing k measurements below 400°C[66].

The oxygen diffusion coefficients (D_O) deduced from these experiments are generally in close agreement, but large scatter of the k values are observed[37,67]. The main reason for this is that it is difficult to make dense samples with a thickness noticeably lower than L_c in order to obtain a surface-limiting process[55]. Consequently, the measurements are carried out in the region of a mixed regime control, and it is difficult to simultaneously determine D* and k* with high accuracy by IEDP method. Various authors have proposed methods to overcome this difficulty and improve confidence for parameter determinations[68-70]. The k* values determined with thin films can be greater than one order of magnitude lower than for bulk samples. Other reasons can be invoked, e.g., k* values found using different techniques are not always comparable[27], the results depend on the thin film synthesis, leading to different materials with the same nominal composition[50,71], and surface segregation effects[72], differences in stress states[73], and strain due to a lattice mismatch between the substrate and the studied film can also affect the outcome[74].

The main inconvenience of these methods is that the characterization conditions of the material do not correspond to their working conditions. Unfortunately, the working conditions of mixed conductors for OTM or SOFC applications are often far from chemical equilibrium. In particular, the system is under a large gradient range of oxygen partial pressure, while in the case of the isotopic exchange method the material is in chemical equilibrium with the surrounding

atmosphere. This could also lead to a significant discrepancy between the performance of materials close to the equilibrium and far from the equilibrium due to the impact of nonlinear phenomena under large gradients of oxygen activity at the surface of mixed conductors[75,76] or to the large variation of kinetic coefficients between the oxygen incorporation and desorption reactions through the oxide/gas interfaces.

This study shows that it is possible to characterize the kinetics of oxygen surface exchanges at the surface of mixed conductors, both near and far from chemical equilibrium, using permeation flux measurements. In both experimental conditions, appropriate modelling allows the acquisition of direct data on the relationship between the oxygen flux and the driving force of oxygen transfer through the gas–solid interface.

2. THEORETICAL BACKGROUND

Oxygen permeation within the framework of the Wagner theory.

Wagner considers that the interface between a gas and a non-stoichiometric material remains in equilibrium even when matter is transferred across the interface. Considering a perovskite material exhibiting a predominant electronic conductivity, i.e., $\sigma_e >> \sigma_{ion}$, according to Wagner[24-26], the permeation flux can be expressed by the following equation:

$$\mathbf{JO_2} = -\frac{\mathrm{RT}}{16\mathbf{F^2}\mathrm{L}} \int_{\mathbf{ln}\,(\mathbf{pO_2^{lean}})}^{\mathbf{ln}\,(\mathbf{pO_2^{rich}})} \boldsymbol{\sigma}_{\mathbf{ion}}\, \boldsymbol{\partial}\mathbf{ln}\,(\mathbf{pO_2}) \qquad (2)$$

JO_2 is the oxygen flux through the membrane (in $mol.m^{-2}.s^{-1}$),

L is the thickness of the membrane,

R is the universal gas constant,

F is the Faraday constant,

pO_2^{rich} is the equivalent oxygen partial pressure in equilibrium with the oxygen-rich surface,

pO_2^{lean} is the equivalent oxygen partial pressure in equilibrium with the oxygen-lean surface, and

T is the absolute temperature.

Two cases can be considered:

- Taking an average value for σ_i or assuming σ_i to be constant simplifies the equation so that JO_2 is directly proportional to σ_i and $\ln(pO_2^{rich}/pO_2^{lean})$[28,77]:

$$JO_2 = \frac{\sigma_i}{16F^2L}\Delta\mu_{O2} = \frac{RT\,\sigma_i}{16F^2L}.\ln\frac{pO_2^{rich}}{pO_2^{lean}} \quad (3)$$

where $\Delta\mu_{O2} = \mu_{O2}^{rich} - \mu_{O2}^{lean} = RT\ln(\frac{pO_2^{rich}}{pO_2^{lean}})$ (4)

- In a simple defect model, neglecting the formation of defect association, the oxygen stoichiometry δ of the oxide material and the ionic conductivity are proportional to $(pO_2)^{1/n}$, i.e., $\delta = \delta^\circ\ (pO_2)^{1/n}$ and $\sigma_i = \sigma_i^\circ\ (pO_2)^{1/n}$. Substitution into Equation (2) with subsequent integration leads to a simplified expression for the oxygen permeation flux:

$$JO_2 = \frac{RT\,n\,\sigma_i^o}{16F^2L}\left((pO_2^{rich})^{\frac{1}{n}} - (pO_2^{lean})^{\frac{1}{n}}\right) \quad (5)$$

where σ_i^o is the value of the ionic conductivity at unit oxygen pressure.

As indicated by Bouwmeester[28], for high values of n, Equation (3) is obtained by expanding Equation (5) as a power series and truncation after the first term.

When pO_2^{rich} is noticeably higher than pO_2^{lean} (which can be neglected), Equation (5) can be simplified as:

$$JO_2 = \frac{RT\, n\, \sigma_i^{o,rich}}{16F^2L} \quad (6)$$

where $\sigma_i^{o,rich}$ is the ionic conductivity of the studied material at the feed pressure, pO_2^{rich}.

From the Nernst-Einstein relationship and equation (3), we obtain:

$$\mathbf{D_O} = -\frac{4RTL}{\mathbf{C_O}\Delta\boldsymbol{\mu_{O2}}}\mathbf{JO_2} \quad (7)$$

where D_O and C_O are the average values of both the oxygen diffusion coefficient through the membrane and the molar concentration of oxygen in the oxide, respectively.

The oxygen diffusion coefficient (D_O) is considered constant over the thickness of the membrane in the steady state, assuming a random distribution of oxygen vacancies in the crystal lattice. In other words, the diffusion coefficient of oxygen measured by the semi-permeation corresponds to the average diffusion coefficient in the range from pO_2^{rich} to pO_2^{lean}. Indeed, this assumption might not hold, when the variation of oxygen activity is large in thickness of the membrane, or under large pO_2 gradient between the both membrane surfaces, as reported usually in the literature.

Limits of the Wagner theory. As recalled in Section 2.1, the Wagner theory assumes that in spite of oxygen transfer through the membrane, both surfaces of the membrane remain in equilibrium with the gas phase. In 1973, Kleitz et al.[48,78] was the first group to experimentally demonstrate that the oxygen permeation flux through a zirconia membrane induces, at high

temperature, a deviation from equilibrium on both sides of the electrolyte. This phenomenon is now generally accepted[28,49,79] and has been recently reviewed[80]. At least three main steps must be considered: i) oxygen diffusion in the gas phase, ii) surface exchange reactions in the adsorbed layers on both sides of the membrane, including adsorption or desorption of oxygen, and iii) bulk diffusion within the membrane. The permeation process is generally a mixed regime that involves bulk diffusion and surface reactions, i.e., adsorption/desorption of oxygen, and the incorporation/extraction of oxygen on both sides of the membrane. Various modelling approaches based on the scheme shown in Figure 1 have been proposed.

The oxygen partial pressure in the vicinity close to the membrane surface (or the corresponding chemical potential of oxygen, referred to as $\mu_{O2\,(g)}^{lean}$ and $\mu_{O2\,(g)}^{rich}$ in Figure 1) can be determined experimentally[81,82] or estimated by computational fluid dynamics simulation[83].

The main difficulty concerns the determination of the actual oxygen activity on the surface of the pellet (or the chemical potential of oxygen, referred to as $\mu_{O2\,(s)}^{lean}$ and $\mu_{O2\,(s)}^{rich}$ in Figure 1). As will be recalled below, we have developed a setup allowing the *in-situ* measurement of the difference between the oxygen chemical potential across the interface at both sides of the membrane (referred to as $\Delta\mu_{O2}^{surf\,(rich)}$ and $\Delta\mu_{O2}^{surf\,(lean)}$ in Figure 1). Consequently, the total oxygen chemical potential variation ($\Delta\mu_{O_2}$) through the membrane is:

$$\Delta\mu_{O_2} = \Delta\mu_{O2}^{bulk} + \Delta\mu_{O2}^{surf\,(rich)} + \Delta\mu_{O2}^{surf\,(lean)} \quad (8)$$

Obviously, in the Wagner theory, both interfaces are assumed to be in equilibrium with the gas ($\Delta\mu_{O2}^{surf\,(rich)}$ and $\Delta\mu_{O2}^{surf\,(lean)}$ are considered as nil), which hinders the proposal of a mechanism for the oxygen transfer through both interfaces. Following the work of Xu and Thomson[84], many

authors have neglected the oxygen chemical potential variation at both interfaces in their modeling equations[85]. By doing this, the equations of the modeling are generally irrelevant[80].

The noticeable deviation from equilibrium at the membrane interfaces often observed in case of transient techniques could explain inconsistencies between the results obtained using the IEDP method vs. relaxation techniques (see Section 4.4).

The expression for the characteristic thickness, L_c, assumes that:

i) The pO_2 gradient through the membrane is small or the surface exchange kinetics are equivalent on both faces of the membrane.

ii) There is a linear relationship between the permeation flux and the oxygen chemical potential gradient through both membrane surfaces. That is, the oxygen chemical potential difference is small (i.e., ($\Delta\mu_{O2}^{surf} \ll RT$), as explained by Kim et al.[40]).

Unfortunately, it has been shown that the surface exchange kinetics at the oxygen-lean and oxygen-rich surfaces are significantly different. Furthermore, the oxygen chemical potential difference on the oxygen-lean surface is significantly larger than RT ($\Delta\mu_{O2}^{surf\,(lean)} \gg RT$)[85].

These relationships between the oxygen flux and the oxygen chemical potential gradient through the membrane are not linear; hence, the definition of the characteristic thickness suggested by Bouwmeester cannot be applied here. The validity of the criterion proposed by Bouwmeester et al. for determining whether bulk diffusion or surface exchange dominate permeation has also been questioned by Yu et al.[87,88]. However, the rate-limiting step of oxygen transport can be easily determined from the oxygen chemical potential profile through the membrane. For example, based

on the similarity to the Biot number in thermal transfer, a critical number denoted as B_c can be directly defined from the oxygen chemical potential gradient through the membrane[89]:

$$B_c = \Delta\mu_{O2}^{surf} / \Delta\mu_{O2}^{bulk} \quad (9)$$

The oxygen flux is governed by oxygen surface exchanges when $B_c \gg 1$, and the oxygen flux is governed by oxygen diffusion when $B_c \ll 1$. A mixed regime can be observed when B_c is close to unity. B^{ox} and B^{red} can then be defined for the oxygen-rich and oxygen-lean surfaces of the membrane, respectively.

Empiric relationships between the permeation flux and oxygen partial pressures on both sides of the membrane have been proposed[28,90,91]. The main drawback of these approaches is that the fitting parameters generally have no physical meaning. Adler et al. suggested a rigorous definition of surface exchange laws in the case of a mixed conductor using a formalism based on the thermodynamics of irreversible processes and mass action laws[75,92]. Starting from this formalism, the relationship below can be established based on the Butler-Volmer equation (Equation (10)). More recently, Bazant had proposed a similar model for ionic species exchange at the solid electrode–electrolyte interface in batteries[76]. From this model, the oxygen flux can be expressed by equation (10) for small or large gradients of oxygen activity through the solid–gas interface.

$$\mathbf{JO_2} = \frac{1}{2}\mathbf{k}\,\mathbf{C_O}\left(\mathbf{e}^{\frac{(1-\beta)\Delta\mu_{O2}^{surf}}{2RT}} - \mathbf{e}^{\frac{-\beta\Delta\mu_{O2}^{surf}}{2RT}}\right) \quad (10)$$

$\mathbf{JO_2}$ is the oxygen flux through the solid–gas interface,

k is the kinetic coefficient of oxygen surface exchange between solid and gas (which depends on the temperature and on the oxygen activity in the solid close to the surface),

C_O is the molar concentration of oxygen in the membrane in the vicinity of its surface,

$\boldsymbol{\Delta\mu_{O2}^{surf}}$ is the difference of the oxygen chemical potential between the gas and the membrane surfaces,

β is a coefficient which takes into account the asymmetric energetic barrier due to the O^{2-} anions crossing a polarized solid–gas interface with an electronic charge transfer. It is usually estimated as 0.5.

The kinetic coefficient of oxygen surface exchange at the both sides of the membrane (oxygen-rich side and oxygen-lean side) can be evaluated using equations (11) and (12):

$$\mathbf{k^{rich}} = \mathbf{2\ JO_2} \Big/ \left(\mathbf{C_0^{rich}} \left(\mathbf{exp}\left(\frac{\mathbf{(1-n)\Delta\mu_{O2}^{surf\ (rich)}}}{\mathbf{2RT}} \right) - \mathbf{exp}\left(\frac{\mathbf{-n\Delta\mu_{O2}^{surf\ (rich)}}}{\mathbf{2RT}} \right) \right) \right) \quad (11)$$

$$\mathbf{k^{lean}} = \mathbf{2\ JO_2} \Big/ \left(\mathbf{C_0^{lean}} \left(\mathbf{exp}\left(\frac{\mathbf{(1-n)\Delta\mu_{O2}^{surf\ (lean)}}}{\mathbf{2RT}} \right) - \mathbf{exp}\left(\frac{\mathbf{-n\Delta\mu_{O2}^{surf\ (lean)}}}{\mathbf{2RT}} \right) \right) \right) \quad (12)$$

where C_O^{rich} and C_O^{lean} are the oxygen molar concentrations in the membrane in the vicinity of the oxygen-rich and oxygen-lean surfaces, respectively.

$\boldsymbol{\Delta\mu_{O2}^{surf\ (rich)}}$ and $\boldsymbol{\Delta\mu_{O2}^{surf\ (lean)}}$ are the differences of the oxygen chemical potential between the gas and the membrane surfaces (see Figure 1). In other words, this term usually corresponds to the driving force of the oxygen flux, also called affinity.

Equation (10) can be simplified by a linear relation (equations (13) and (14)) if $\Delta\mu_{O2}^{surf} << 2$ RT.

$$JO_2 = k\, C_O\, \frac{\Delta\mu_{O2}^{surf}}{4RT} \quad (13)$$

and

$$k = \frac{4RT}{C_O \, \Delta\mu_{O2}^{surf}} JO_2 \qquad (14)$$

In this study, the oxygen semi-permeation measurements were carried out near and far from equilibrium at the solid–gas interface, which involves differentiating the oxygen adsorption/insertion process from the desorption reactions at each sample face (reactions 1 and 2, respectively)[75] as follows:

$\frac{1}{2}\, O_{2\,(g)} + V_O^{\bullet\bullet} \xrightarrow{k_i} O_O^X + 2\,h^{\bullet}$ reaction 1 : the adsorption/insertion step at the oxygen-rich face,

$O_O^X + 2\,h^{\bullet} \xrightarrow{k_d} \frac{1}{2}\, O_{2\,(g)} + V_O^{\bullet\bullet}$ reaction 2 : the desorption step at the oxygen-lean face.

In other words, k^{rich} and k^{lean} can be associated with the kinetic coefficients of the oxygen incorporation (k_i) and desorption (k_d) steps, respectively.

3. OXYGEN PERMEATION MEASUREMENTS

Measurement of the variation of the oxygen chemical potential at the membrane surface. The setup for the *in-situ* measurement of the oxygen chemical potential variation has been described in various publications[49,84,93]. The scheme of the cell is given in Figure 2. Two micro-probes were gently pressed on either side of the membrane surface: a metallic gold electrode (Au), and a ceramic tip (yttria-stabilized zirconia (YSZ) or yttria-doped ceria (YDC)), which consists of a cone-shaped ceramic probe (approximately 3 mm in diameter and 3–5 mm in height) with a platinum coating on the top of the probe. The ceramic microtips can be machined from a ceramic

rod or made thanks to recent developments in additive manufacturing technologies. For instance, the zirconia microtips were obtained by stereolithography (SL).

As demonstrated previously[48,94], on both sides of the membrane, the emf between the microelectrodes obeys the following equation (15) (see Figure 2):

$$E = \frac{(\mu_{O_2\,(g)} - \mu_{O_2\,(s)})}{4\,F} = \frac{\Delta\mu_{O_2}^{surf}}{4\,F} \qquad (15)$$

The yttria-stabilized zirconia or ceria-based electrolyte microtips must be small to avoid the systemic error linked to the oxygen activity gradients in the gas close to the membrane surface[80,86].

Oxygen semi-permeation setup under high oxygen gradients. The basic oxygen semi-permeation setup is composed of three chambers, as schematized in Figure 3. The lateral chamber (chamber 3) is required to prevent eventual oxygen leakage through the gold sealing, and two opposite chambers with different oxygen partial pressures in the flowing inert gases allow the creation of an oxygen chemical potential gradient between the two faces of the disk membrane. Chamber 1 corresponds to the sample face in contact with an oxygen-rich atmosphere, while chamber 2 corresponds to the sample face swept by the oxygen-lean gas mixture.

The difference of oxygen chemical potential in the gas phase on both sides of the membrane ($\Delta\mu_{O2}$) is measured from the oxygen partial pressure in the gas outlet of chambers 1 and 2 (see equation 16) using the zirconia oxygen sensors; J2 and J3, respectively.

$$\Delta\mu_{O2} = \mu_{O2\,(g)}^{rich} - \mu_{O2\,(g)}^{lean} = RT\ln\left(\frac{pO_{2\,(ch.1)}}{pO_{2\,(ch.2)}}\right) \qquad (16)$$

$\mu_{O2\,(g)}^{rich}$: oxygen chemical potential in the gas in chamber 1 (oxygen-rich atmosphere),

$\mu_{O2\,(g)}^{lean}$: oxygen chemical potential in the gas in chamber 2 (oxygen-lean atmosphere),

$pO_{2\,(ch.1)}$: oxygen partial pressure in the gas in chamber 1, measured by a zirconia oxygen sensor (J3),

$pO_{2\,(ch.2)}$: oxygen partial pressure in the gas in chamber 2, measured by a zirconia oxygen sensor (J2).

The specific oxygen semi-permeation flux, (JO_2) through the sample is calculated from the variation of the oxygen partial pressure in the outlet gas from chamber 2, as shown in equation (17):

$$JO_2 = \frac{f_g\,(P_{2out}\text{-}P_{2in})}{S\,V_m} \qquad (17)$$

where f_g is the sweep flow rate (10 $mL.min^{-1}$) in chamber 1,

V_m is the molar volume of gas at room temperature ($L.mol^{-1}$),

S is the efficient membrane surface (m^2),

P_{2in} is the oxygen partial pressure in the inlet gas of chamber 2, measured using the zirconia sensor J1,

and P_{2out} is the oxygen partial pressure in the outlet gas from chamber 2, measured using the zirconia sensor J2.

The difference of oxygen chemical potential between the membrane surface and the gas, at both sides of the pellet, is determined from the electromotive forces between a gold microelectrode and the ceria cone-shaped microelectrode in contact with the membrane surface (Figure 3). It is then

possible to evaluate the oxygen chemical potential difference through the bulk of the disk membrane, $\Delta\mu_{O2}^{bulk}$, from equation (18).

$$\Delta\mu_{O2}^{bulk} = \Delta\mu_{O2} - \Delta\mu_{O2}^{surf\,(rich)} - \Delta\mu_{O2}^{surf\,(lean)} \quad (18)$$

Oxygen semi-permeation setup under low-oxygen gradients. A few setups have been proposed for studying the permeation process under low-oxygen gradients. The pressure difference between the membrane surfaces was kept very small to minimize the difference between the corresponding values of the stoichiometry ratio (δ) on the opposite sides of the pellet and, moreover, to allow consideration of the permeation flows proportional to $\Delta\mu_{O2}^{bulk}$ (see equation (13)). The experimental approach proposed by Patrakeev et al.[95,96] and developed further by Kharton and Figueiredo involves a cell with independent electrochemical devices for measuring and pumping oxygen[97,98]. The cells consist of three separate parts: a tubular zirconia oxygen electrochemical pump, a disk-shaped zirconia oxygen sensor, and the ceramic membrane under study. The two disks, sample and sensor, were sealed to the pump using an appropriate glass, which formed a gastight chamber[98]. This construction was chosen in order to prevent the voltage applied to the electrodes of the oxygen pump from affecting the sensor emf reading[97,99,100]. For a given oxygen pressure within the chamber (controlled by the sensor emf), the permeation flux density is determined by the current passing through the oxygen pump. Notably, the quality of the sealing is a critical issue to be taken into consideration[100]. Moreover, even with low oxygen potential gradients, the overvoltage at both interfaces cannot always be neglected[79].

Daslet et al.[101] have proposed a combination of a local ceramic probe and a closed cell, which allows the application of a small, steady state, oxygen chemical potential difference across the membrane, ensuring an almost homogenous oxide ion distribution. The oxygen flux is proportional

to the current passing through the pump. Furthermore, relaxation measurements can be made using a stepwise gas composition change on one side of the membrane. However, as in other proposed setups[101,103], the sensor and oxygen pump are located on the same zirconia pellet, which induces an electrical-coupling effect between the oxygen sensor and the pump. Moreover, diffusional limitations may appear when the small inner volume of the cell contains a mixture of oxygen and inert gas. This drawback can be partially avoided by blowing pure oxygen through the cell before the sample is sealed[104].

Our proposed setup for measuring very low oxygen permeation fluxes under low oxygen partial pressure gradients is schematized in Figure 4.

The inlet oxygen partial pressure in chamber 2 is controlled by two mass flowmeters (Brooks) between 1-20 $mL.min^{-1}$ for nitrogen gas and 1-10 $mL.min^{-1}$ for air. The resulting low flowrate through chamber 2 is favorable for obtaining a significant variation in the oxygen partial pressure in the gas outlet of chamber 2 despite a very low oxygen semi-permeation flux through the disk sample. In this work, the gas flowrate in chamber 2 was fixed to 10 $mL.min^{-1}$.

To prevent electromagnetic perturbations, the cell furnace was supplied with DC current using a stabilized power supply[105]; to reduce the electrical pick-up, the experimental cell and the sensors were shielded by a grounded platinum layer coated on the external surface of an alumina tube.

The specific configuration of this setup allows for obtaining a very high accuracy in the measurement of the oxygen semi-permeation flux and of the oxygen activity gradient at the membrane surface. In particular, the low gas flowrate in chamber 2 (10 $ml.min^{-1}$) and the low oxygen gradient between both faces reduce the systemic error due to the oxygen activity gradient in gas in the vicinity of the membrane, as reported in previous studies[83,86].

As shown in Figure 4, the difference of the oxygen chemical potential in the gas phase ($\Delta\mu_{O2}^{total}$) between chambers 1 and 2 can be controlled by adding oxygen or air to the gas flow, which is controlled by a mass flowmeter (Brook, 0-10 ml.min^{-1}), referred to as D3 in Figure 5. In these conditions, the oxygen permeation flux obeys the following equation:

$$JO_2 = \frac{f_g\,(P_{2S}-P_{2S0})}{S\,V_m} \qquad (22)$$

where P_{2S} is the partial pressure of oxygen in the outlet gas from chamber 2 when the difference of oxygen pressure between chamber 1 and 2 is not zero, and P_{2S0} is the partial pressure of oxygen in the outlet gas from chamber 2 when the difference of oxygen partial pressure-between chamber 1 and 2 is equal to zero. P_{2S} and P_{2S0} are measured via the oxygen zirconia sensor in the outlet gas flow of chamber 2 (J2 sensor in Figure 4).

In the next section, we show that the evaluations of $\Delta\mu_{O2}^{bulk}$, $\Delta\mu_{O2}^{surf\,(rich)}$ and $\Delta\mu_{O2}^{surf\,(lean)}$ enable the determination of the oxygen diffusion coefficient (D_O), oxygen incorporation coefficient (k_i) and oxygen desorption coefficient (k_d), respectively.

4. RESULTS AND DISCUSSION

Oxygen chemical potential gradient through the $La_{0.6}Sr_{0.4}Co_{0.2}Fe_{0.8}O_{3-\delta}$ perovskite (LSCF6428) membrane sample.

Information dealing with the LSCF6428 sample preparation is given in additional content (S1). The profile of the oxygen chemical potential through the LSCF6428 membrane clearly identifies the nature of the limiting step of oxygen transport by determining the B_c values (Table

1). The semi-permeation oxygen measurements were performed at 900°C, and the difference of oxygen partial pressure between chambers 1 and 2 was fixed at a constant value of pO_2' / pO_2" ≈ 2.2, in four successive oxygen partial pressure ranges (pO_2' and pO_2'' in atm.): 0.48/0.21, 0.11/4.7. 10^{-2}, 2.8. 10^{-2}/1.3. 10^{-2}, and 6.3. 10^{-3}/3. 10^{-3} atm.

Figure 5 depicts the variation of the oxygen chemical potential through the LSCF6428 membrane according to the three main steps of oxygen transport:

1) Oxygen diffusion through the bulk of the membrane,

2) Oxygen surface exchange (or the oxygen incorporation step) at the oxygen-rich surface,

3) Oxygen surface exchange (or the oxygen desorption step) at the oxygen-lean surface.

Figure 5 shows that for a similar oxygen chemical potential gradient between chambers 1 and 2 ($\Delta\mu O_2 = RT \ln (P_{O_2}^{rich}/P_{O_2}^{lean}) = 8$ kJ.mol^{-1}), the difference of chemical potential of oxygen at the oxygen-lean surface ($\Delta\mu_{O2}^{surf\,(lean)}$) markedly decreases with the oxygen partial pressures. On the opposite side, the oxygen chemical potential gradient though the bulk of the membrane ($\Delta\mu_{O2}^{bulk}$) increases with the oxygen partial pressure. This means that the step that limits the oxygen flux through the membrane largely depends on the oxygen partial pressure on the both side of the membrane: the oxygen flux through the sample is governed by the bulk oxygen diffusion at high pO_2 (> 0.2 atm.) and by oxygen desorption at low pO_2 (< 0.03 atm.).

Relationship between driving force and oxygen flux. The specific oxygen semi-permeation method reported in the present work allows, on the one hand, controlling the driving force, and the other hand, measuring the oxygen flux through the membrane or through both

membrane surfaces, with very high accuracy. This leads to experimentally establishing the relationship between the driving force (i.e., the difference of oxygen chemical potential) and the oxygen flux for small or large oxygen chemical potential gradients (i.e., near and far from equilibrium). It is then possible to determine the validity domain of the conventional linear relationship between oxygen flux and the driving force for small oxygen chemical potential differences. The setup also can be used to evaluate the oxygen pressure limits of this approximation owing to the large variation in the oxygen vacancy concentration in the materials with the surrounding oxygen partial pressure. In contrast, the isotopic exchange method does not allow working far from the chemical equilibrium, and it does not take into account the eventual nonlinear behavior under a large oxygen activity gradient through the membrane surface.

Figures 6 a and b show the variation of the oxygen flux as a function of the driving force (or gradient of oxygen chemical potential), under a high oxygen partial pressure range (close to 0.21 atm.) and a low oxygen partial pressure range (close to 0.02 atm.), respectively. As expected, a linear relationship under small oxygen chemical potential gradients is obtained under low and high oxygen partial pressures (0.21 and 0.02 atm.).

The linear behavior is expected when the difference of oxygen chemical potential is low: i.e. $\Delta\mu_{O2}^{surf} \ll RT$ or $\frac{\Delta\mu_{O2}^{surf}}{RT} \ll 1$ (if number of oxygen transfer in rate determining step = 2), as reported in previous works[106,107] and in agreement with equation (10)[76,108]. When the oxygen chemical potential differences $\left(\Delta\mu_{O2}^{surf}\right)$ increases at the surface, the nonlinear behavior is more marked at low oxygen partial pressures (see Figure 6 b, e.g., 0.02 atm.). This feature demonstrates that it is important to evaluate the oxygen surface coefficients under a small oxygen chemical potential gradient, because the linearity between the driving force and the oxygen permeation flux

is assumed for the determination of both the oxygen surface exchange coefficients and the oxygen diffusion coefficient.

At low pO_2, under a large $\Delta\mu_{O2}^{surf\,(lean)}$, the J_{O_2} variation is not linear (when $\frac{\Delta\mu_{O2}^{surf\,(lean)}}{RT}$ is higher than 0.5, see triangular plots on figure 6 b), this nonlinear behavior could be linked to the large variation in the k_i and k_d coefficients when the pO_2 increases, as reported in a previous work[108]. Under high pO_2, the opposite situation arises: $\Delta\mu_{O2}^{surf\,(lean)}$ is too low ($\frac{\Delta\mu_{O2}^{surf\,(lean)}}{RT} < 0.2$, see triangular plots on figure 6 a), and a linear behavior between the driving force and the oxygen flux was observed, because the surface is close to equilibrium with the surrounding atmosphere at the vicinity of the surface membrane.

Besides, these results also clearly confirm that the oxygen incorporation reaction is faster than the oxygen desorption or oxygen release reaction ($k_i > k_d$), in particular at low pO_2. Similar trends have been observed in the literature: the oxidation steps are systematically quicker than the corresponding reduction steps using the ECR method[23–26,37,109,110]. This effect may be due to the nonlinear pO_2-dependence of k_{chem}. In order to keep the deviation as small as possible, the pO_2 steps in the current study were performed under conditions close to the equilibrium.

Indeed, the values of k (or k_{chem}) are very sensitive to the operating conditions of the measurements, which has led to the large scatter in k (or k_{chem}) values in the literature (see Figure S2 in associated content). In particular, the nonlinear pO_2 dependence of k (or k_{chem}) can lead to a large variation in the k_{chem} or k values if the measurement of k is performed close to the equilibrium (corresponding to a small oxygen activity gradient) or far from equilibrium (corresponding to a large oxygen activity gradient). The current study also shows that the determination of oxygen diffusion and

surface exchange coefficients of mixed ionic-electronic conductors requires the use of a small oxygen activity gradient due to the coefficients being dependent on the pO_2, as reported in the next section.

D_O, k_i and k_d are dependent on the oxygen partial pressure. The oxygen semi-permeation measurements were performed at 900°C, and the oxygen partial pressure in chamber 2 was fixed at three successive values: 0.2, 10^{-2}, and 10^{-3} atm. Figure 7 shows that the oxygen diffusion coefficient, oxygen incorporation coefficient at the oxygen-rich surface and the oxygen desorption coefficient at the oxygen-lean surface are dependent on the pO_2 value.

Figure 7 shows that the values of D_O, k_i and k_d obtained by the semi-permeation method at 900°C under a small oxygen activity gradient are lower than the values of D* and k* evaluated at 900°C by the isotopic exchange method for similar perovskite materials[37,111]. The D_O coefficient at 900°C is slightly lower than the D* coefficient evaluated in the literature. The D_O/D* ratio is close to 0.6-0.7, which corresponds to the correlation factor that is often reported in the literature for the perovskite structure (H = 0.69).

The k* value at 900°C (from data reported in the literature (Figure 8 b)) is significantly higher than the k_i and k_d coefficients obtained in this work at the same temperature; this discrepancy cannot be explained by the impact of the correlation factor only. We assumed here that the discrepancy was linked to the impact on the values of k*, k_i and k_d of the surface preparation or microstructure of the sample. For instance, previous works show that the surface physical-chemistry[112-114] and grain sise[115,116] has a large impact on the values of oxygen incorporation or desorption coefficients of $La_{0.5}Sr_{0.5}Fe_{0.7}Ga_{0.3}O_{3-\delta}$ perovskite or yttria-stabilized zirconia (YSZ).

This could explain the large discrepancy between the values obtained in the literature for powder and for large bulk samples of the same composition, as observed by Fielitz et al.[120].

One of the advantages of the oxygen semi-permeation technique in comparison with other methods is that it allows dissociating the oxygen incorporation and desorption steps via determining the k_i and k_d coefficients directly on thick bulk samples and close to the operating conditions (and not on powders).

The n coefficients reported in Figure 7 and Table 2 were deduced from the slopes of the straight lines in Figure 8, which correspond to the exponential coefficient in the following equation (23) and from previously reported results.

$$k = k_0(pO_2)^n \quad (23)$$

Figure 7 shows the significant variation of n values between the oxygen incorporation step and the oxygen desorption step. This assumes that the predominant oxygen mechanism at the membrane surface could be different for the incorporation and desorption mechanisms, as reported in Table 2.

However, the n values in the literature for similar material compositions vary from 0.45 to 0.74[37, 43,117]. The values obtained in the current study are lower, with 0.27 for k_i and 0.54 for k_d. This assumes that the pO_2 dependence of k or the limiting step of oxygen transport through the solid–gas interface can also be affected by the physicochemical properties of materials[114], in particular by the density of the grain boundary or the eventual presence of secondary phases in the grain boundaries at the material surface[116].

D_O, k_i, and k_d are dependent on temperature. The oxygen semi-permeation measurements were performed at 800°C, 850°C, 900°C, 950°C, and 1000°C. This temperature range enables significant oxygen fluxes through the membrane under a low oxygen activity gradient. The oxygen partial pressure in chamber 2 remained near 0.2 atm, and the oxygen partial pressure in chamber 1 was fixed close to 0.45 atm for each temperature. Figure 8 shows that the oxygen diffusion coefficient (D_O), oxygen incorporation coefficient (k_i) and oxygen desorption coefficient (k_d) are temperature dependent. Unfortunately, at lower temperatures (< 800°C), the oxygen flux measurement is not accurate enough to correctly evaluate D_O and k_i and k_d, which are ± 30 % and ± 15 %, respectively, at 900°C.

The activation energy of the oxygen diffusion coefficient is nearly 150 kJ.mol^{-1}, and those of the oxygen incorporation and desorption are close to 160 and 200 kJ.mol^{-1}, respectively. These values are very similar as those reported in previous studies, e.g., E_a = 145 kJ.mol^{-1} for bulk diffusion and 178 kJ.mol^{-1} for the surface exchange[116]. Furthermore, Elshof et al.[43] reported that the activation energy of the oxygen diffusion coefficient is in the range of 140-165 kJ.mol^{-1} for $La_{0.6}Sr_{0.4}Co_{0.4}Fe_{0.6}O_{3-\delta}$ perovskite materials, and Berenov et al.[119] demonstrated a similar activation energy (145 kJ.mol^{-1}) for $La_{0.6}Sr_{0.4}CoO_{3-\delta}$ perovskite materials.

In contrast, as shown in Figure 8 b, the scatter of both of the published k* values and of the corresponding activation energies is very large. No explanation was given regarding the very low values of k* measured by the IIE technique for powders[56,57] compared with the values determined for bulk samples by the IEDP method. Moreover, there is a large range of reported activation energies (E_a) of k* in the literature [117], from 32 to 250 kJ.mol^{-1} for the same $La_xSr_{1-x}Co_{1-y}Fe_yO_{3-\delta}$ perovskite material series. Notably, the activation energy value of k* for $La_{0.6}Sr_{0.4}CoO_{3-\delta}$ perovskite (73 kJ.mol^{-1} (0.76 eV)[110,117] was significantly lower than that reported in this study (190

kJ.mol^{-1} (1.97 eV)). This variation could mainly be linked to the impact of the cobalt ratio in $La_xSr_{1-x}Co_{1-y}Fe_yO_{3-\delta}$ perovskite on the E_a value for the surface exchange mechanism. However, Armstrong et al.[56,57] found very small positive apparent activation energies of the surface exchange coefficients on perovskite powders and high activation energy values for oxide pellets using the IEDP technique. Using the ECR technique with porous perovskite, Ganeshananthan et al.[39] found very small positive and even negative apparent activation energies of the surface exchange coefficient. Several explanations have been proposed, e.g., difficulty in the simultaneous determination of k* and D by fitting the experimental curves for a single measurement[44] and variation of the oxygen surface coverage with temperature[39, 56,117]. In this context, Fielitz et al. [120] recently proposed a novel interpretation of the boundary conditions for a mixed controlled regime, in contradiction with the study by Maier[27], who assumed that the surface is close to chemical equilibrium. We believe that these discrepancies could be ascribed to the large difference in the physicochemical properties of the actual surface[114] between a powder and a dense sintered sample of the same material composition due to the grain size[116]. For instance, the density of grain boundaries on the sample surface can have a strong impact on the oxygen surface exchange mechanisms[111,115]. Indeed, the sample preparation (polishing of surface) or the operating conditions (as the water partial pressure) leads to a large effect on the kinetics of oxygen surface exchange, as reported by various authors [112,122–124], and this could explain the large variation of k* values reported in the literature for the same material composition.

5. CONCLUSION

This study shows that it is possible to determinate the oxygen diffusion and oxygen exchange surface coefficients for mixed ionic-electronic conductors, with suitable accuracy, by the oxygen semi-permeation method. However, this method requires a significant oxygen flux though the

membrane sample to obtain a suitable accuracy of the oxygen diffusion and oxygen surface exchange coefficients. This involves determining these transport coefficients at higher temperatures (> 800°C) in comparison to those required in the isotopic method (usually < 900°C).

However, the main advantage of the oxygen semi-permeation method is the ability to quickly determine the oxygen diffusion and oxygen surface coefficients in a single measurement that is close to the working conditions, i.e., close or far from the equilibrium. This also allows the identification of the relationship between oxygen flux and the driving force, for which there is very few data in the literature. Finally, this method offers new data, and it could give new perspectives for better understanding oxygen surface exchange mechanisms that are near and far from the equilibrium at the surface of mixed ionic or electronic conductors.

Supplementary Material

Listing of the contents:

S1: Sample preparation of $La_{0.6}Sr_{0.4}Fe_{0.8}Co_{0.2}O_{3-\delta}$ perovskite

S2: pO_2 dependence on the k_{chem} coefficient

S1) Sample preparation of $La_{0.6}Sr_{0.4}Co_{0.2}Fe_{0.8}O_{3-\delta}$ perovskite

The $La_{0.6}Sr_{0.4}Co_{0.2}Fe_{0.8}O_{3-\delta}$ (LSCF6428) powders were synthesized using the nitrate-citrate route. The oxygen semi-permeation measurements require a dense disk sample with a thickness of 1-2 mm and a diameter of 23-24 mm. The disk samples were produced by the tape casting process, as previously reported [aa]. The green samples were debinded at 1°C.min^{-1} in air and sintered at 1250°C for 4 hours. The relative density of LSCF6428 sample have been more 0.95. The faces of LSCF6428 sample are polished with successive grades of silicon carbide abrasive paper and finally polished with alumina down to ¼ micron.

[aa] P.-M. Geffroy, M. Reichmann, L. Kilmann, J. Jouin, N. Richet, and T. Chartier, *J. Membr. Sci.*, **476**, 340 (2015).

S2) pO_2 dependence on k_{chem} values

Figure S2. pO_2 dependence on k_{chem} values from different work reported in the literature.

[a] J. A. Lane, S. J. Benson, D. Waller, and J. A. Kilner, *Solid State Ionics*, **121**, 201 (1999).

[b] H. J. M. Bouwmeester, M. W. Van den Otter, and B. A. Boukamp, *J. Solid State Electrochem.*, 8, 599 (**2004**).

[c] Y. L. Huang, C. Pellegrinelli, K. T. Lee, A. Perel, and E.D. Wachsman, *J. Electrochem. Soc.*, **162**, F965 (2015).

[d] A. Cox-Galhotra, S. McInstosh, *Solid State Ionics*, **181**, 1429 (2010).

[e] J. A. Lane, J. A. Kilner, *Solid State Ionics*, **136–137**, 997 (2000).

AUTHOR INFORMATION

Corresponding Author

*Dr. Pierre-Marie Geffroy,

E-mail: pierre-marie.geffroy@unilim.fr

IRCER, CNRS, Université de Limoges, CEC, 12 Rue Atlantis 87068 Limoges, France

Author Contributions

The manuscript was written through contributions of all authors. All authors have given approval to the final version of the manuscript. ‡These authors contributed equally. (match statement to author names with a symbol)

ACKNOWLEDGMENTS

The authors would like to thank the Region Limousin for financial supports. The authors would like to thanks also Nicolas Lory for technical help in the development of new oxygen semi-permeation setup working under low gradients of oxygen activity.

ABBREVIATIONS

SOFC, Solid oxide fuel cell; SOEC, Solid oxide electrolysis cell; OTM, oxygen transport membrane; MIEC, Mixed ionic-electronic conductor; IEDP, Isotopic exchange depth profile method; SIMS, Secondary ion mass spectrometry; ECR, Electrical conductivity relaxation method; IIE, Isothermal isotopic exchange method; PIE, Pulse-response ^{18}O–^{16}O isotope exchange method; YSZ, Yttria-stabilized zirconia;, YDC, Yttria-doped ceria; SL, Stereolithography; LSCF6428, $La_{0.6}Sr_{0.4}Co_{0.2}Fe_{0.8}O_{3-\delta}$ perovskite.

REFERENCES

(1) U. Balachandran, B. Ma, P. S. Maiya, R. L. Mieville, J. T. Dusek, J. J. Picciolo, J. Guan , S. E. Dorris, and M. Liu, *Solid State Ionics*, **108**, 363 (1998).

(2) V. V. Kharton, E. N. Naumovich, and A. V. Nikolaev, *J. Membr. Sci.,* **111**, 149 (1996).

(3) S. Baumann, W. A. Meulenberg, and H. P. Buchkremer, *J. Eur. Ceram. Soc.*, **33**, 1251 (2013).

(4) C.-Y. Tsai, A. G. Dixon, W. R. Moser, and Y. H. Ma , *AIChE J.*, **43**, 2741 (1997).

(5) H. J. M. Bouwmeester, *Catal. Today*, **82**, 141(2003).

(6) A. Thursfield, and I. S. Metcalfe, *J. Mater. Chem.*, **14**, 2475 (2004).

(7) W. Q. Jin, S. G. Li, P. Huang, N. P. Xu, J. Shi, and Y. S. Lin, *J. Membr. Sci.*, **166**, 13 (2000).

(8) T. Wall, Y. Liu, C. Spero, L. Elliott, S. Khare, R. Rathnam, F. Zeenathal, B. Moghtaderi, B. Buhre, C. Sheng, R. Gupta, T. Yamada, K. Makino, J. Yu, *Chem. Eng. Res. Des.*, **87**, 1003 (2009).

(9) M. Ni, M. K. H. Leung, and D. Y. C. Leung, *Int. J. Hydrogen Energy*, **33**, 2337 (2008).

(10) S. H. Morejudo, R. Zanón, S. Escolástico, I. Yuste-Tirados, H. Malerød-Fjeld, P. K. Vestre, W.G. Coors, A. Martínez, T. Norby, J. M. Serra, and C. Kjølseth, *Science,* **353***,* 563 (2016).

(11) C. Chatzichristodoulou, M. Søgaard, And P. V. Hendriksen, *J. Electrochem. Soc.*, **158** (5), F61 (2011).

(12) Y. Y. Liu, X. Y. Tan, and K. Li, *Catal. Rev. Sci. Eng.*, **48**, 145 (2006).

(13) M. H. R. Lankhort, H. J. M. Bouwmeester, and H. Verweij, *J. Am. Ceram. Soc.*, **80**, 2175 (1997).

(14) C. Li, J. J. Chew, A. Mahmoud, S. Liu, and J. Sunarso, *J. Membr. Sci.*, **567**, 228 (2018).

(15) J. Fouletier, H. Seinera, and M. Kleitz, *J. Appl. Electrochem.*, **5**, 177 (1975).

(16) K. L. Duncan, K.-T. Lee, and E. D. Wachsman, *J. Power Sources*, **196**, 2445 (2011).

(17) J. M. Serra, V. B. Vert, O. Büchler, W. A. Meulenberg, and H. P. Buchkremer, *Chem. Mater.*, **20**, 3867 (2008).

(18) J. Fouletier and V. Ghetta, *Solid State Electrochemistry I: Fundamentals, Materials and their Applications*, V. V. Kharton, Editor, p. 397, Wiley-VCH, Weinheim (2009).

(19) P. Fabry, M. Kleitz, and C. Déportes, *J. Solid State Chem.*, **5**, 1 (1972) (in French).

(20) V. V. Kharton and F. M. B. Marques, *Solid State Ionics*, **140**, 381 (2001).

(21) V. V. Kharton, A. P. Viskup, F. M. Figueiredo, E. N. Naumovich, A. A. Yaremchenko, and F. M. B. Marques, *Electrochim. Acta*, **46**, 2879 (2001).

(22) V. V. Kharton, A. L. Shaula, N. P. Vyshatko, and F. M. B. Marques, *Electrochim. Acta*, **48**, 1817 (2003).

(23) J. R. Frade, V. V. Kharton, A. A. Yaremchenko, and E. V. Tsipis, *J. Solid State Electrochem.*, **10**, 96 (2006).

(24) C. Wagner C., *Proceedings of International Comm. Electrochem. Thermo. and Kinetics (CITCE)*, 7th Meeting, Lindau, 1955, p. 361, Butterworth Sci. Publ., London, (1957).

(25) C. Wagner C., *Progress in Solid State Chemistry*, **10**, 3 (1975).

(26) L. Heyne, *Solid Electrolytes, Topics in Applied Physics*, S. Geller (Editor), p. 169, Springer, Berlin, (1977).

(27) J. Maier, *Solid State Ionics*, **112**, 197 (1998).

(28) H. J. M. Bouwmeester, H. Kruidhof, and A. J. Burggraaf, *Solid State Ionics*, **72**, 185 (1994).

(29) H. J. M. Bouwmeester and A. J. Burggraaf, *The CRC Handbook of Solid State Electrochemistry*, P. J. Gellings and H. J. M. Bouwmeester, Editors, p. 481, CRC Press, London, (1997).

(30) J. E. ten Elshof, H. J. M. Bouwmeester, and H. Verweij, *Solid State Ionics*, **81**, 97 (1995).

(31) R. J. Chater, S. Carter, J. A. Kilner, and B. C. H. Steele, *Solid State Ionics*, **53**, 859 (1992).

(32) J. A. Kilner, B. C. H. Steele, and L. Ilkov, *Solid State Ionics*, **12**, 89 (1984).

(33) J. A. Kilner, R. A. De Souza, and I. C. Fullarton, *Solid State Ionics*, **86–88**, 703 (1996).

(34) J.-M. Bassat, M. Petitjean, J. Fouletier, C. Lalanne, G. Caboche, F. Mauvy, and J.-C. Grenier, *Applied Catalysis A: General*, **289**, 84 (2005).

(35) E. Boehm, J.-M. Bassat, P. Dordor, F. Mauvy, J.-C. Grenier, and Ph. Stevens, *Solid State Sciences*, **176**, 2717 (2005).

(36) R. H. E. Van Doorn, I. C. Fullarton, R. A. De Souza, J. A. Kilner, H. J. M. Bouwmeester, and A. J. Burggraaf, *Solid State Ionics*, **96**, 1 (1997).

(37) J. A. Lane, S. J. Benson, D. Waller, and J. A. Kilner, *Solid State Ionics*, **121**, 201 (1999).

(38) S. Wang, P. A. W. Van der Heide, C. Chavez, A. J. Jacobson, and S. B. Adler, *Solid State Ionics*, **156**, 201 (2003).

(39) R. Ganeshananthan and A. V. Virkar, *J. Electrochem. Soc.*, **152**, A1620 (2005).

(40) S. Kim, Y. L. Yang, A. J. Jacobson, and B. Abeles, *Solid State Ionics*, **121**, 31 (1999).

(41) M. Mosleh, M. Søgaard, and P. Vang Hendriksen, *J. Electrochem. Soc.*, **156** (4), B441 (2009).

(42) A. Zomorrodian, H. Salamati, Z. G. Lu, X. Chen, N. J. Wu, and A. Ignatiev, *Int. J. Hydrogen Energy*, **35**, 12443 (2010).

(43) J. E. ten Elshof , M. H. R. Lankhorst, and H. J. M. Bouwmeester, *J. Electrochem. Soc.*, **144**, 1060 (1997).

(44) A. Cox-Galhotra and S. McInstosh, *Solid State Ionics*, **181**, 1429 (2010).

(45) F. Mauvy, J.-M. Bassat, E. Boehm, P. Dordor, J.-C. Grenier, and J.-P. Loup, *J. Europ. Ceram. Soc.*, **24**, 1265 (2004).

(46) T. Hong, L. Zhang, F. Chen, and C. Xia, *J. Power Sources*, **218**, 254 (2012).

(47) F. Mauvy, E. Boehm, J.-M. Bassat, J.-C. Grenier, and J. Fouletier, *Solid State Ionics*, **178**, 1200 (2007).

(48) J. Fouletier, P. Fabry, and M. Kleitz, *J. Electrochem. Soc.*, **123**, 204 (1976).

(49) C.-S. Chen, Z.-P. Zhang, G.-S. Jiang, C.-G. Fan, W. Liu, and H. J. M. Bouwmeester, *Chem. Mater.*, **13**, 2797 (2001).

(50) Y. H. Li, K. Gerdes, T. Horita, and X. B. Liu, *J. Electrochem. Soc.*, **160**, F343 (2013).

(51) T. M. Huber, E. Navickas, K. Sasaki, B. Yildiz, H. Tuller, G. Friedbacher, H. Hutter, and J. Fleig, *J. Electrochem. Soc.*, **164** (7), F809 (2017).

(52) M. Sahibzada, W. Morton, A. Hartley, D. Mantzavinos, and I. S. Metcalfe, *Solid State Ionics*, **136-137**, 991 (2000).

(53) N. Knoblauch, L. Dörrer, P. Fielitz, M. Schmücker, and G. Borchardt, *Phys. Chem. Chem. Phys*., **17**, 5849 (2015).

(54) C. Crank, The mathematics of diffusion, 2nd Edn., Clarendon Press, Oxford, 1975, p. 44.

(55) C. C. Kan, H. H. Kan, F. M. Van Assche, E. N. Armstrong , and E. D. Wachsman, *J. Electrochem. Soc.*, **155** (10), B985 (2008).

(56) E. N. Armstrong, K. L. Duncan, and E. D. Wachsman, *Phys. Chem. Chem. Phys.*, **15**, 2298 (2013).

(57) E. N. Armstrong, K. L. Duncan K. L., D. J. Oh, J. F. Weaver, and E. D. Wachsman, *J. Electrochem. Soc.*, **158** (5), B492 (2011).

(58) H. J. M. Bouwmeester, C. Song, J. Zhu, J. Yi, M. Van Sint Annaland, and B.A. Boukamp, *Phys. Chem. Chem. Phys.*, **11**, 9640 (2009).

(59) C.-Y. Yoo, B. A. Boukamp, and H. J. M. Bouwmeester, *J. Solid State Electrochem.*, **15**, 231 (2011).

(60) C.-Y. Yoo, H. J. M. Bouwmeester, *Phys. Chem. Chem. Phys.*, **14**, 11759 (2012).

(61) A. Esquirol, N. P. Brandon, J. A. Kilner, and M. Mogensen, *J. Electrochem. Soc*., **151** (11), A1847 (2004).

(62) M. Guillodo, J.-M. Bassat, J. Fouletier, L. Dessemond, and P. Del Gallo, *Solid State Ionics*, **164**, 87 (2003).

(63) M. Mogensen and S. Skaarup, *Solid State Ionics*, **86-88**, 1151 (1996).

(64) C. Endler-Schuck, J. Joos, C. Niedrig, A. Weber, and E. Ivers-Tiffée, *Solid State Ionics*, **269**, 67 (2015).

(65) J. Laurencin, M. Hubert, K. Couturier, T. Le Bihan, P. Cloetens, F. Lefebvre-Joud, and E. Siebert, *Electrochimica Acta*, **174**, 1299 (2015).

(66) Q. Yang and J. D. Nicholas, *J. Electrochem. Soc.,* **161** (11), F3025 (2014).

(67) R. A. De Souza, *Phys. Chem. Chem. Phys.,* **8**, 890 (2006).

(68) P. Fielitz and G. Borchardt, *Solid State Ionics*, **144**, 71 (2001).

(69) F. Ciucci, *Solid State Ionics*, **239**, 28 (2013).

(70) J. Blair and D. S. Mebane, *Solid State Ionics*, **270**, 47 (2015).

(71) Y. L. Yang, A. J. Jacobson, C. L. Chen, G. P. Luo, K. D. Ross, and C. W. Chu, *Appl. Phys. Lett.*, **79**, 776 (2001).

(72) A. Karthikeyan and S. Ramanathan, *Appl. Phys. Lett*., **92**, 243109 (2008).

(73) Q. Yang, T. E. Burye, R. R. Lunt, and J. D. Nicholas, *Solid State Ionics*, **249–250**, 123 (2013).

(74) M. M. Kuklja, E. A. Kotomin, R. Merkle, A. Mastrikov, and J. Maier, *Phys. Chem. Chem. Phys*., **15**, 5443 (2013).

(75) S. B. Adler, X/ Y. Chen, and J. R. Wilson, *J. Catal*., **245**, 91 (2007).

(76) M. Z. Bazant, *Accounts of Chemical Research,* **46**, 1144 (2013).

(77) L. Qiu, T. H. Lee, L.-M. Liu, Y. L. Yang, and A. J. Jacobson, *Solid State Ionics*, **76**, 321 (1995).

(78) M. Kleitz, P. Fabry, E. Schouler, *Fast Ion Transport in Solids*, W. van Gool, Editor, p. 439, North Holland Pub. Co, Amsterdam (1973).

(79) F. M. Figueiredo, F. M. B. Marques, and J. R. Frade, Electrochemical permeability of $La_{1-x}Sr_xCoO_{3-\delta}$ materials, *Solid State Ionics*, **11**, 273 (1998).

(80) M. C. Steil, J. Fouletier, and P.-M. Geffroy, *J. Membr. Sci*., **541**, 457 (2017).

(81) A. Hunt, G. Dimitrakopoulos, P. Kirchen, and A. F. Ghoniem, *J. Membr. Sci*., **468**, 62 (2014).

(82) A. Hunt, G. Dimitrakopoulos, and A. F. Ghoniem, *J. Membr. Sci*., **489**, 248 (2015).

(83) W. Chen, N. Nauels, H. J. M. Bouwmeester, A. Nijmeijer, and L. Winnubst, *J. Europ. Ceram. Soc.*, **35**, 3075 (2015).

(84) S. J. Xu and W. J. Thomson, *Chem. Eng. Sci.*, **54**, 3839 (1999).

(85) G. Dimitrakopoulos and A. F. Ghoniem, *J. Membr. Sci.*, **510**, 209 (2016).

(86) P.-M. Geffroy, A. Vivet, J. Fouletier, C. Steil, E. Blond, N. Richet, P. Del Gallo, and T. Chartier, *J. Electrochem. Soc.*, **160**, F60 (2013).

(87) A. S. Yu, J. M. Vohs, and R. J. Gorte, Energy Environ. Sci., **7**, 944 (2014).

(88) A. S. Yu, J. Kim, T.-S. Oh, G. Kim, R. J. Gorte, and J. M. Vohs, Appl. Catal. A, **486**, 259 (2014).

(89) O. Valentin, E. Blond, and N. Richet, *Adv. Sci. Techn.*, **65**, 232 (2010).

(90) H. J. M. Bouwmeester, H. Kruidhof, A. J. Burggraaf, and P. J. Gellings, *Solid State Ionics*, **53–56**, 460 (1992).

(91) S. Dou, C. R. Masson, and P. D. Pacey, *J. Electrochem. Soc*., **132**, 1843 (1985).

(92) Y. Cao, M. J. Gadre, A. T. Ngo, S. B. Adler, and D. D. Morgan, *Nature Communications*, **10: 1346**, 1 (2019).

(93) M. Guillodo, J. Fouletier, L. Dessemond, and P. Del Gallo, *J. Electrochem. Soc.*, **149**, 93 (2002).

(94) F. Mauvy and J. Fouletier, Stoichiometry and Materials Science - When Numbers Matter, A. Innocenti and N. Kamarulzaman, Editors, chap. 7, p. 175, InTech, (2012).

(95) M. V. Patrakeev, I. A. Leonidov, V. L. Kozhevnikov, V. I. Tsidilkovskii, A. K. Demin, and A. V. Nikolaev, *Solid State Ionics*, **82**, 61 (1993).

(96) M. V. Patrakeev, I. A. Leonidov, and V. L. Kozhevnikov, *Solid State Ionics*, **82**, 5 (1995).

(97) V. V. Kharton, A. P. Viskup, E. N. Naumovich, and F. M. B. Marques, *J. Mater. Chem.*, **9**, 2623 (1999).

(98) F. M. Figueiredo, V. V. Kharton, J. C. Waerenborgh, A. P. Viskup, E. N. Naumovich, and J. R. Frade, *J. Am. Ceram. Soc.*, **87**, 2252 (2004).

(99) J. Fouletier, G. Vitter, and M. Kleitz, *J. Appl. Electrochem.*, **5**, 111 (1975).

(100) F. M. Figueiredo, J. R. Frade, and F. M. B. Marques, *Solid State Ionics*, **110**, 45 (1998).

(101) B. T. Daslet, M. Søgaard, and P. V. Hendriksen, *J. Electrochem. Soc.*, **154**, B1276 (2007).

(102) V. V. Kharton, E. N. Naumovich, and A. V. Nikolaev, *Solid State Ionics*, 83, 301 (1996).

(103) E. Ivers-Tiffée, C. Niedrig, and S. F. Wagner, *ECS Transactions*, **61**, 283 (2014).

(104) V. V. Kharton, A. P. Viskup, E. N. Naumovich, and N. M. Lapchuk, *Solid State Ionics*, **104**, 67 (1997).

(105) J. Fouletier, M. Bonnat, J. Le Bot, and S. Adamowicz, *Sensors Actuators B*, **45**, 155 (1997).

(106) M. Leonhart, R.A. De Souza, J. Claus, and J. Maier, *J. Electrochem. Soc.,* **149**, J19 (2002).

(107) J. Maier, *J. Am. Ceram. Soc.*, **76**, 1212 (1993).

(108) P.-M. Geffroy, L. Guironnet, H. J. M. Bouwmeester, T. Chartier T., J.-C. Grenier, and J.-M. Bassat, *J. Europ. Ceram. Soc.*, **39**, 59 (2019).

(109) E. Bucher, W. Sitte, F. Klauser, and E. Bertel, *Solid State Ionics*, **19**, 61 (2011).

(110) S. Wang, A. Verma, Y. L. Yang, A. J. Jacobson, and B. Abeles, *Solid State Ionics*, **140**, 125 (2001).

(111) R. A. De Souza and J. A. Kilner, *Solid State Ionics*, **106**, 175 (1998).

(112) M. J. Pietrowski, R. A. De Souza, M. Fartmann, R. ter Veen, M. Martin, *Fuel Cells*, **5,** 673 (2013).

(113) H. Kusaba, Y. Shibata, K. Sasaki, Y. Teraoka, *Solid State Ionics*, **177,** 2249 (2006).

(114) L. Guironnet, P.-M. Geffroy, N. Tessier-Doyen, A. Boulle, N. Richet, and T. Chartier, *J. Membr. Sci.*, **588**, 117 (2019).

(115) R. A. De Souza, M. J. Pietrowski, U. Anselmi-Tamburini, S. Kim, Z. A. Munir, and M. Martin, *Phys. Chem. Chem. Phys.*, **10**, 2067 (2008).

(116) P.-M. Geffroy, E. Blond, N. Richet, and T. Chartier, *Chem. Engin. Sci.*, **162**, 245 (2017).

(117) Y. L. Huang, C. Pellegrinelli, K. T. Lee, A. Perel, and E. D. Wachsman, Enhancement of $La_{0.6}Sr_{0.4}Co_{0.2}Fe_{0.8}O_{3-\delta}$ Surface Exchange through Ion Implantation, *J. Electrochem. Soc.,* **162**, F965 (2015).

(118) S. J. Benson, Oxygen Transport and Degradation Processes in Mixed Conducting Oxides, PhD thesis, Imperial College, (1999).

(119) A. V. Berenov, A. Atkinson, J. A. Kilner, E. Bucher, and W. Sitte, *Solid State Ionics*, **181**, 819 (2010).

(120) P. Fielitz and G. Borchard, *Phys. Chem. Chem. Phys.,* **18**, 22031 (2016).

(121) S. J. Benson, R. J. Chater, J. A. Kilner, and B. C. H. Steele, in *3rd Ionic and Mixed Conducting Ceramics III*, T. A. Ramanarayanan, W. L. Worrell, H. L. Tuller, A. C. Khandkar, M. Mogensen, and W. Göpel, Editors, p. 596, The Electrochem. Soc. Proc. Series, Pennington, NJ (1997).

(122) A. Atkinson, R.J. Chater, and R. Rudkin, *Solid State Ionics*, **139**, 233 (2001).

(123) R. N. Vannier, S. J. Skinner, R. J. Chater, J. A. Kilner, and G. Mairesse, *Solid State Ionics*, **160**, 85 (2003).

(124) N. Sakai, K. Yamaji, T. Horita, Y. P. Xiong, H. Kishimoto, and H. Yokokawa, *J. Electrochem. Soc.*, **150**, A689 (2003).

Table 1. Evolution of the limiting step of oxygen transport through the LSCF6428 membrane, according to pO_2.

pO_2 conditions Chamber 1/ 2 (pO_2^{rich} / pO_2^{lean} in atm)	$B_c^{(rich)}$	$B_c^{(lean)}$	Limiting step of oxygen transport
0.48/0.21	0.1	0.3	Bulk oxygen diffusion
0.11/0.047	0.24	1.2	Mixed regime
0.028/0.013	0.75	4	Oxygen desorption
0.006/0.003	3.2	14	Oxygen desorption

Table 2: Evolution of the n coefficient reported in equation 23.

Compounds	pO_2 range (atm)	Reference		n
LSCF6428	0.6/0.03	This work	k_i	0.27
LSCF6428	0.6/0.03	This work	k_d	0.54
LSCF6428	1/0.01	Lane-Benson[37]	k*	0.45
LSCF6428	0.2/0.025	Huang et al.[117]	k*	0.7
LSCF6428	1/0.005	Benson-Chater[121]	k*	0.74

Figure captions

Figure 1. Schematic variation of the oxygen chemical potential across a permeating MIEC membrane.

Figure 2. Schematic drawing of the electrochemical cell allowing the measurement of oxygen activity on both surfaces of a MIEC.

Figure 3. Oxygen semi-permeation setup working with a large oxygen activity gradient, as reported in previous works.

Figure 4. Oxygen semi-permeation setup working with a low-oxygen activity gradient, used in this work.

Figure 5. Oxygen chemical potential profiles through the $La_{0.6}Sr_{0.4}Co_{0.2}Fe_{0.8}O_{3-\delta}$ (LSCFCo6428) 1mm thick membrane at 900°C, for a constant oxygen partial pressure gradient through the cell, pO_2' / pO_2" ≈ 2.2, of between 3. 10^{-3} and 0.48 atm.

Figure 6. Variation of the permeation flux at 900°C as a function of the driving force for the three main steps of oxygen transport through the membrane: oxygen incorporation, oxygen desorption, and oxygen bulk diffusion a) for oxygen pressures close to 0.21 atm. and b) for oxygen pressures close to 0.02 atm. (we assume in this work that the temperature have low impact on the energy activation of k* and D* in this range of temperature).

Figure 7. Variation of the diffusion and surface exchange coefficients with the oxygen partial pressure, $La_{0.6}Sr_{0.4}Co_{0.2}Fe_{0.8}O_{3-\delta}$ (LSCF6428) sample (1 mm thick) at 900°C, from 3. 10^{-3} to 0.5 atm. The values of D* and k* were obtained by the isotopic exchange method[37] for the same

material composition at 800°C and evaluated at 900°C from E_a = 160 kJ.mol^{-1} for k* and E_a = 200 kJ.mol^{-1} for D*, respectively.

Figure 8. Temperature dependence, from 800 to 1000°C, of a) oxygen diffusion coefficient (D_O), b) oxygen incorporation coefficient (k_i) and oxygen desorption coefficient (k_d) of $La_{0.6}Sr_{0.4}Co_{0.2}Fe_{0.8}O_{3-\delta}$ materials.

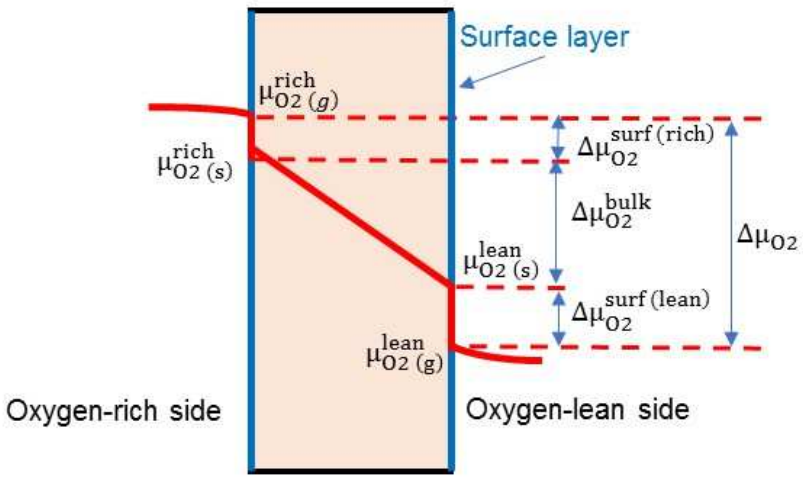

Figure 1. Schematic variation of the oxygen chemical potential across a permeating MIEC membrane.

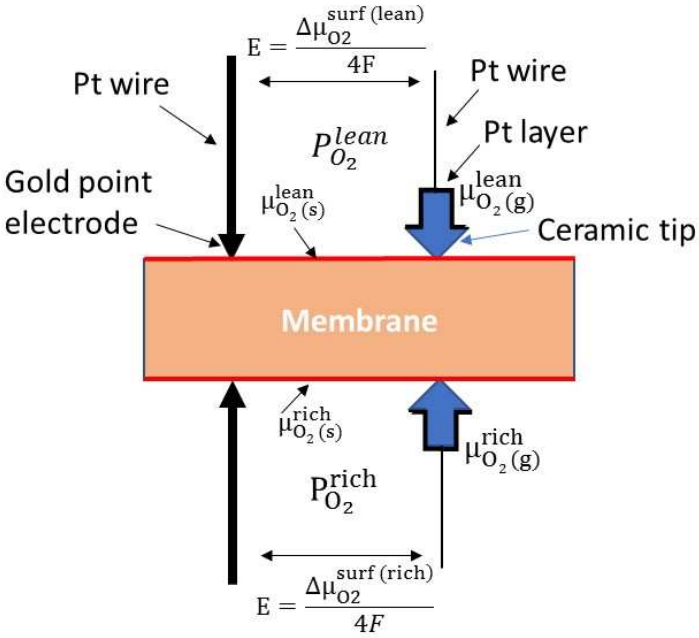

Figure 2. Schematic drawing of the electrochemical cell allowing the measurement of oxygen activity on both surfaces of a MIEC.

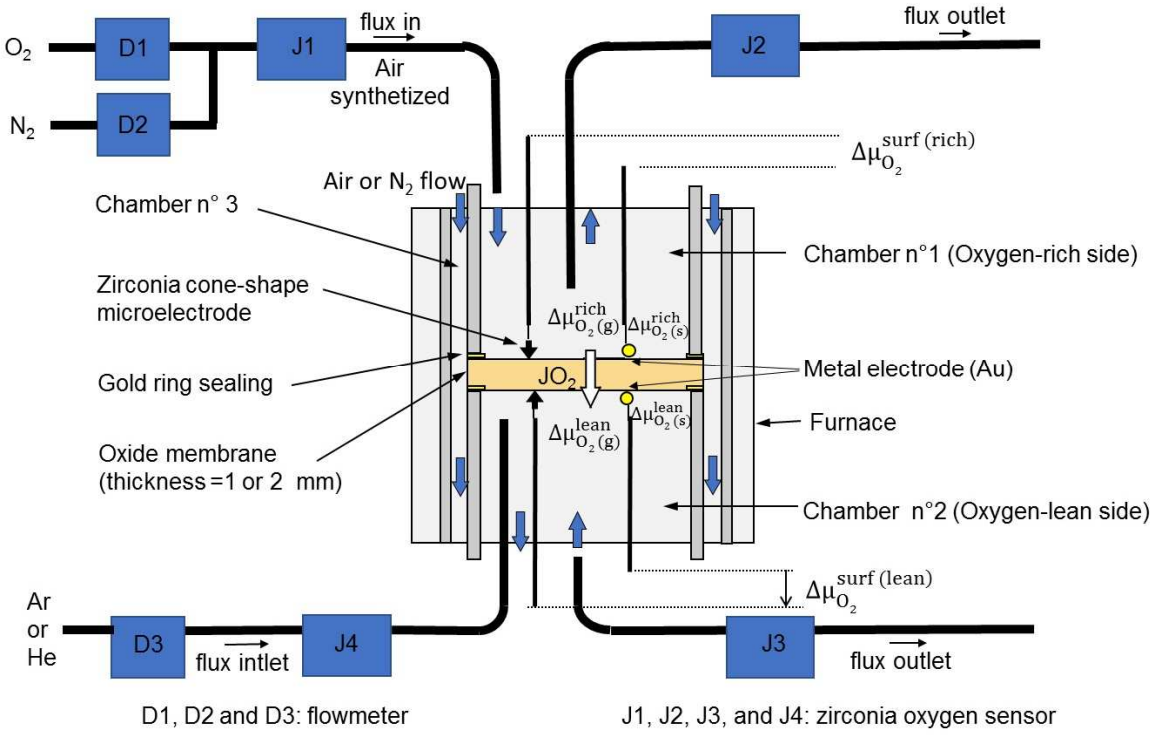

Figure 3. Oxygen semi-permeation setup working with a large oxygen activity gradient, as reported in previous works.

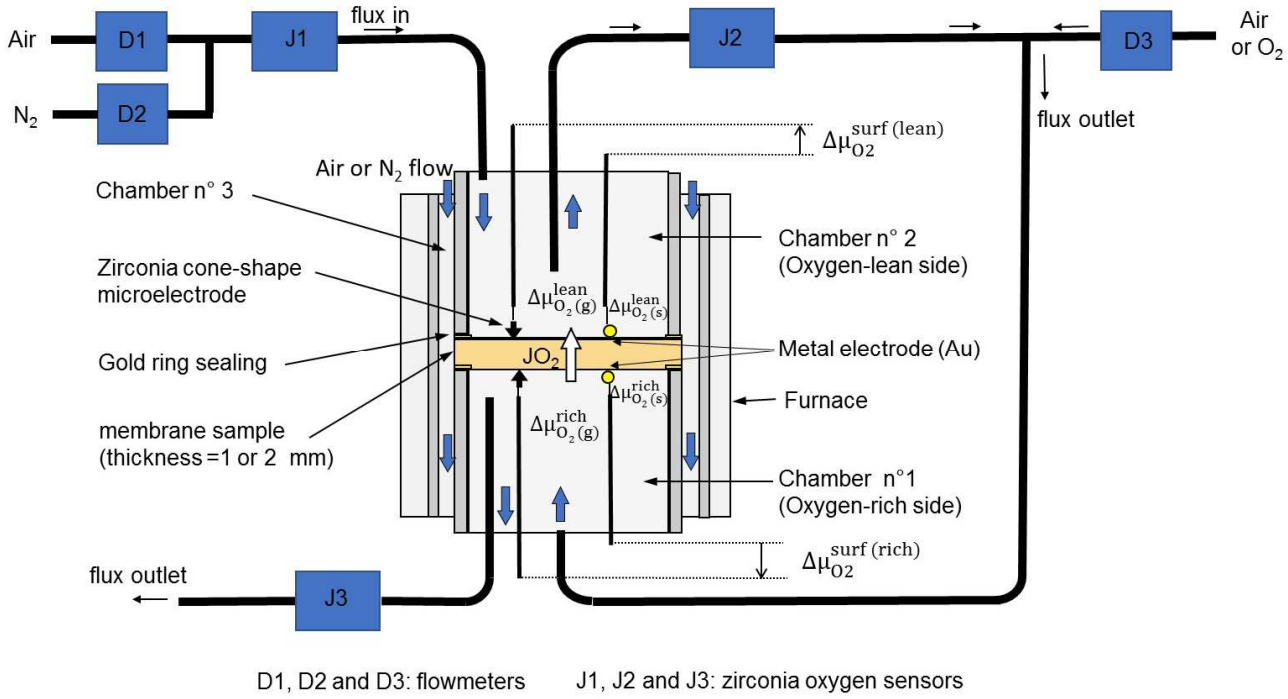

Figure 4. Oxygen semi-permeation setup working with a low-oxygen activity gradient used in this work.

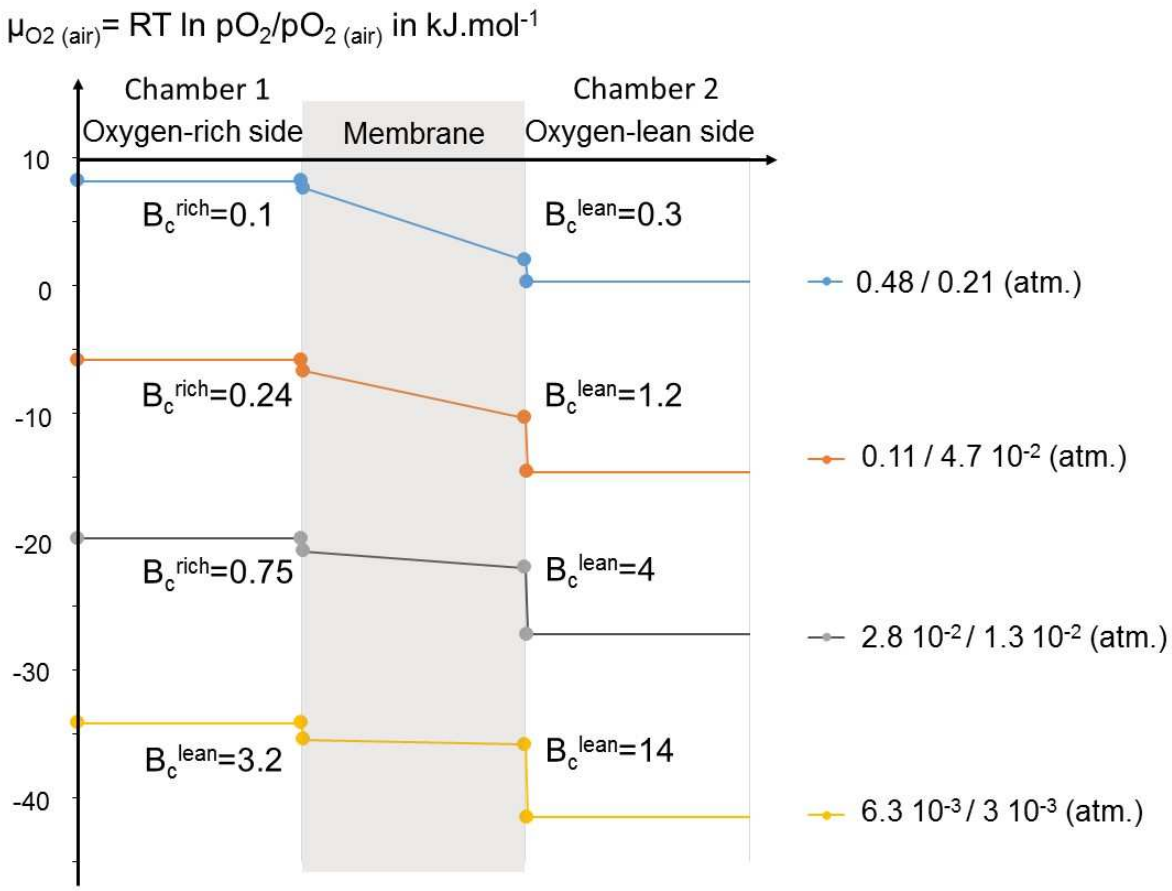

Figure 5. Oxygen chemical potential profiles through the $La_{0.6}Sr_{0.4}Co_{0.2}Fe_{0.8}O_{3-\delta}$ (LSCF6428) 1mm thick membrane at 900°C, for a constant oxygen partial pressure gradient through the cell, pO_2' / pO_2" ≈ 2.2, of between 3. 10^{-3} and 0.48 atm.

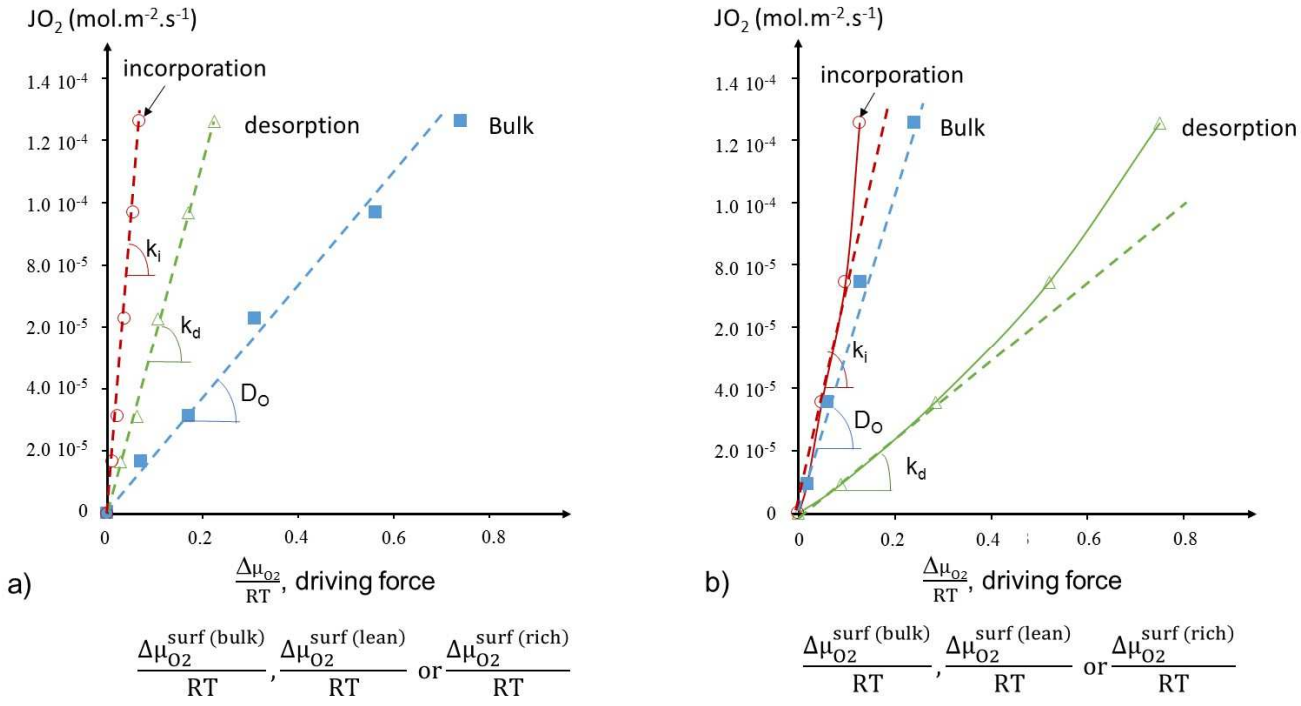

Figure 6. Variation of the permeation flux at 900°C as a function of the driving force for the three main steps of oxygen transport through the membrane: oxygen incorporation, oxygen desorption, and oxygen bulk diffusion a) for oxygen pressures close to 0.21 atm and b) for oxygen pressures close to 0.02 atm.

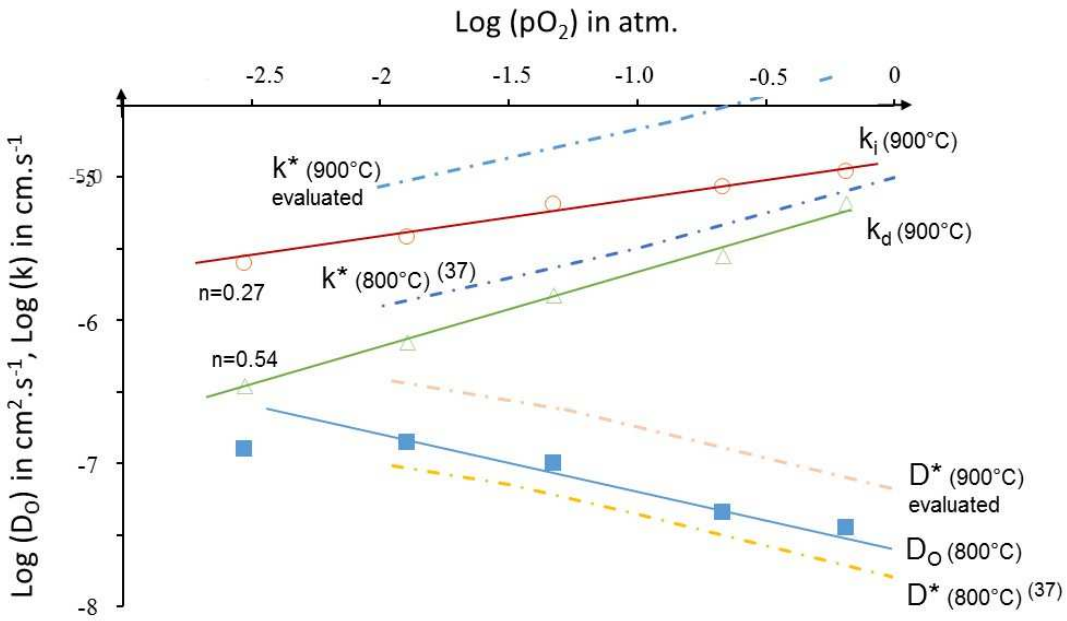

Figure 7. Variation of the diffusion and surface exchange coefficients with the oxygen partial pressure, $La_{0.6}Sr_{0.4}Co_{0.2}Fe_{0.8}O_{3-\delta}$ (LSCF6428) sample (1 mm thick) at 900°C, from 3. 10^{-3} to 0.5 atm. The values of D* and k* were obtained by the isotopic exchange method[37] for the same material composition at 800°C and evaluated at 900°C from E_a = 160 kJ.mol^{-1} for k* and E_a = 200 kJ.mol^{-1} for D*, respectively (we assume in this work that the temperature have low impact on the activation energy of k* and D* in this range of temperature).

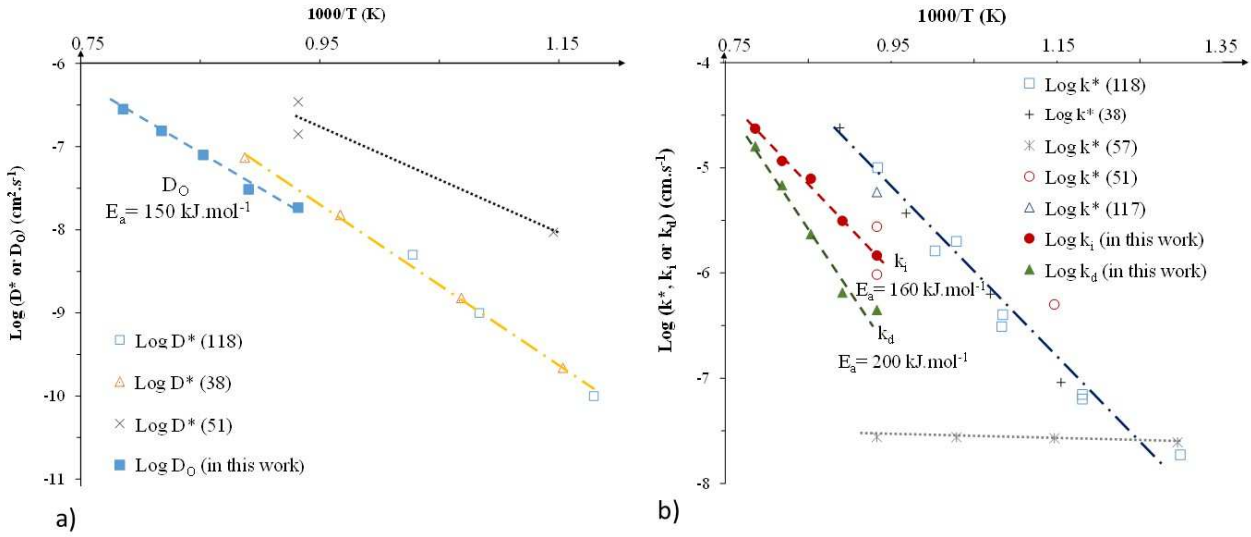

Figure 8. Temperature dependence, from 800 to 1000°C, of a) oxygen diffusion (D_O), b) oxygen incorporation coefficient (k_i) and oxygen desorption coefficient (k_d) of $La_{0.6}Sr_{0.4}Co_{0.2}Fe_{0.8}O_{3-\delta}$ materials.